

Multi-component reactive transport modeling of natural attenuation of an acid groundwater plume at a uranium mill tailings site

Chen Zhu^{a,*}, Fang Q. Hu^a, David S. Burden^b

^a *Old Dominion University, Norfolk, VA 23529, USA*

^b *U.S. Environmental Protection Agency, National Risk Management Research Laboratory, Ada, OK 74820, USA*

Received 10 December 1999; received in revised form 7 April 2000; accepted 20 April 2000

Abstract

Natural attenuation of an acidic plume in the aquifer underneath a uranium mill tailings pond in Wyoming, USA was simulated using the multi-component reactive transport code PHREEQC. A one-dimensional model was constructed for the site and the model included advective–dispersive transport, aqueous speciation of 11 components, and precipitation–dissolution of six minerals. Transport simulation was performed for a reclamation scenario in which the source of acidic seepage will be terminated after 5 years and the plume will then be flushed by uncontaminated upgradient groundwater. Simulations show that successive pH buffer reactions with calcite, $\text{Al}(\text{OH})_3(\text{a})$, and $\text{Fe}(\text{OH})_3(\text{a})$ create distinct geochemical zones and most reactions occur at the boundaries of geochemical zones. The complex interplay of physical transport processes and chemical reactions produce multiple concentration waves. For SO_4^{2-} transport, the concentration waves are related to advection–dispersion, and gypsum precipitation and dissolution. Wave speeds from numerical simulations compare well to an analytical solution for wave propagation. © 2001 Elsevier Science B.V. All rights reserved.

Keywords: Geochemical modeling; Contaminant; Transport; Coupled processes

1. Introduction

Accurate prediction of the fate and transport of regulated metals and radionuclides in the subsurface of abandoned mining sites is critical to the assessment of environmental

* Corresponding author. Present address: Department of Geology and Planetary Science, University of Pittsburgh, Pittsburgh, PA 15260. Tel.: +1-412-624-8780.

E-mail address: czhu@pitt.edu (C. Zhu).

impact and to the development of effective remediation technologies. However, this task has been almost exclusively addressed, in industrial practice, by the use of K_d -based “reactive” transport models. K_d or linear isotherm, as well as Langmuir and Freundlich isotherms, are phenomenological and empirical parameters. Although K_d -based transport models are mathematically simple, it is well known that they are insufficient to describe the complex geochemical reactions that control the distribution of solutes between groundwater and aquifer matrix in subsurface environments (Stumm and Morgan, 1981; Reardon, 1981; Bethke and Brady, 2000). In the case of active or abandoned mining sites with acid mine drainage problems, the shortcomings of this approach become more severe because

(1) Precipitation–dissolution reactions dominate the attenuation of some solutes. Because the solubility products control the reactions but the mass of the solids plays no part in the solubility product constraints, no continuously differentiable isotherms relate solid and fluid concentrations for precipitation–dissolution reactions (Bryant et al., 1987);

(2) The single retardation factor approach fails to consider the interactions among multiple solutes. These interactions are important in the transport of some contaminants. For example, the precipitation of gypsum, which retards the transport of sulfate in groundwater in acid mine drainage systems, results from the rise of the activity of calcium in groundwater due to calcite dissolution. Calcite dissolution is in turn a result of the transport of protons;

(3) The seepage of acidic fluid into even a homogenous aquifer will produce chemical zonations or heterogeneity, which also evolves spatially through time. Thus, it is impossible to have a constant K_d or to know the variation of K_d values with time and space a priori.

A more promising approach to the simulation of reactions and flow in chemically complex and heterogeneous environments is the use of *coupled reactive transport models* in which the advective–dispersive transport equations are solved together, either simultaneously or sequentially, with the mass-action and mass-balance equations for chemical reactions (Schwartz and Domenico, 1973; Walsh, 1983; Cederberg et al., 1985; Lichtner, 1985; Yeh and Tripathi, 1989, 1991; Steefel and Lasaga, 1994; Raffensperger and Garven, 1995). Dozens of coupled reactive transport models have been developed in the past 20 years (see reviews by Mangold and Tsang, 1991; Zhu et al., 1996). However, applications of coupled reactive transport models to abandoned mining sites are scarce. Yeh and Tripathi (1991) applied the model HYDROGEOCHEM to a “synthetic” uranium mill-tailings site and incorporated limited chemistry. Walter et al. (1994b) applied MINTRAN to a “generic” abandoned mining site, resembling the Nordic mine uranium mill tailings site near Elliot Lake, Northern Ontario. Glynn and Brown (1996) described preliminary results of application of the PHREEQC model to the Pinal Creek site in Arizona. Despite the seriousness of the acid mine drainage problem (cf. King, 1995), the chemical reactions and chemical evolution in the aquifers as a result of seepage of acidic fluids are poorly understood.

In this study, natural attenuation of a contaminated aquifer in an abandoned uranium mill tailings site in Wyoming, USA was simulated using the U.S. Geological Survey multi-component reactive transport code PHREEQC version 2.0 (Parkhurst and Appello,

1999). A recent study of this site (the Bear Creek Uranium site) has collected a large amount of hydrological and geochemical data (Zhu et al., 2001). This study thus allows the development of a more complex and detailed reactive transport model than possible in previous studies. Modeling results were qualitatively compared to field data and analyzed in terms of concentration wave propagation.

2. Site contamination and hydrogeological setting

The Bear Creek Uranium site is located in the southern part of the Powder River Basin in Wyoming (Fig. 1). A uranium mill operated from the 1970s to the mid-1980s. Sulfuric acid and sodium chlorate were used to dissolve and oxidize uranium. Spent acids and tailings slurries were piped to unlined tailings ponds. An estimated 3.3 million tons of tailings and 880 million gallons of liquid effluent have been disposed into the

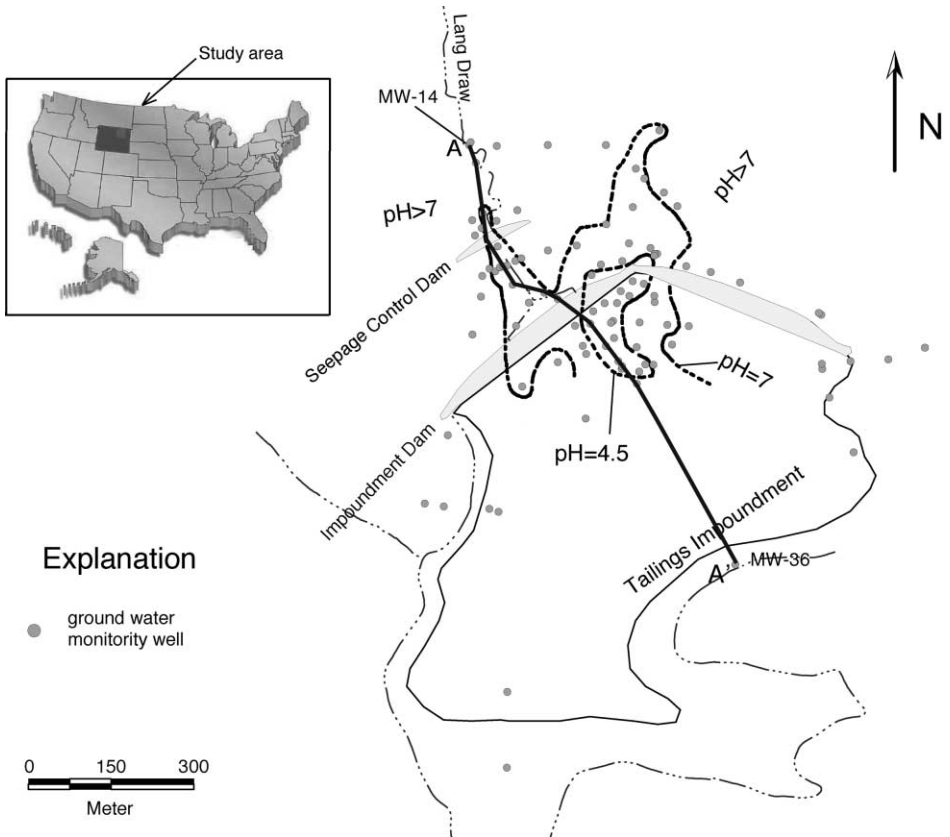


Fig. 1. Plan view of the mine site and tailings impoundment. The dashed lines are pH contours, which delineate the flow paths at the site.

tailings pond. The tailings fluid has a pH between 1.5 and 3.5, a total dissolved solid (TDS) content close to 20,000 mg/l, and high concentrations of arsenic (As), beryllium (Be), cadmium (Cd), chromium (Cr), lead (Pb), molybdenum (Mo), nickel (Ni), selenium (Se), radium (^{226}Ra , ^{228}Ra), thorium (^{230}Th), and uranium (U).

Seepage from the disposal ponds into the underlying N sand of the Eocene Upper Wasatch Formation and alluvium aquifer has formed an acid plume (Fig. 2). The N sand and alluvium at the site is comprised primarily of quartz, microcline, a small amount of plagioclase, and about 2 wt.% calcite (Sharp and Gibbons, 1964; Zhu et al., 2001). Measured total iron concentration in the Wasatch Formation is about 0.4 wt.% as Fe (Sharp and Gibbons, 1964). Groundwater occurs 3 to 8 m below land surface. Numerous aquifer tests have been performed to evaluate transmissivities and storage coefficients. The hydraulic conductivity for the alluvium at Lang Draw is estimated at 3 m/day and for N sand beneath the tailings impoundments is 0.9 m/day (GeoTrans, 1987, 1995, unpublished reports). A groundwater flow model was developed and modeling results show that groundwater flows preferentially in the alluvium along Lang Draw, where the permeability is high, and to the northeast from the bend of the Impoundment Dam (GeoTrans, 1987, 1995, unpublished reports). These flow paths are supported by groundwater pH data, which outline the plume of lower pH groundwater (Fig. 1). Regional groundwater flows from the south of the site beneath the tailings basin and to the north. The estimated pre-mining regional groundwater gradient is 0.014 m/m.

To contain the migration of the plume downgradient, low-pH water was pumped from wells installed along the Lang Draw downgradient from the impoundment dam and piped into constructed evaporation basins within the tailings impoundment. Over time, the efficiency of these pumping wells has decreased significantly. The current reclamation plan is to install a low-permeability cover on the tailings ponds to prevent further infiltration from precipitation. Results from hydrological modeling show that tailings

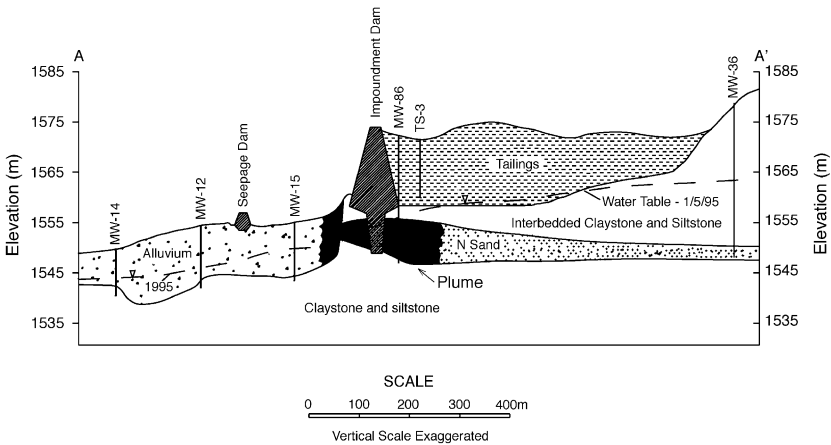


Fig. 2. Cross-section A–A' from Fig. 1. It also shows the names and locations of the monitoring wells discussed in the text. Shaded area in the aquifer represents the estimated extent of the low-pH plume.

pore water will cease to drain into the underlying N sand 5 years after the cover installation. After that time, the plume will be flushed by uncontaminated upgradient groundwater. The distance of the migration of the acid plume and regulated metals and radionuclides will depend on the “natural attenuation” or the reactions of aquifer minerals with contaminated groundwater. The coupled reactive transport model is designed to simulate the acid plume migration under this “cover and attenuate” reclamation plan.

3. Model description

An 800-m strip along cross-section A–A' (Fig. 2) was discretized into 200 cells (Fig. 3). Each cell is 4 m in length. The model starts at the southern end of the pH 4.5 zone in the N sand and extends to near the property boundary. Grid size sensitivity analysis was performed by varying the grid size from 1 to 10 m, while keeping other parameters the same (time steps also changed accordingly). The results from these simulations show that the differences are indiscernible. For the base case, the time step is 0.08 year.

A uniform and constant Darcy velocity of 15 m/year and effective porosity of 0.3 were used along the entire cross-section. The tailings fluid has high chloride concentrations (0.016 mol/l), while the background water has only 0.0007 mol/l. It is widely believed that Cl^- acts as a conservative solute in most aquifer systems and thus, its distribution can be used to retrieve dispersivity for the aquifer. By trial and error, a longitudinal dispersivity between 10 and 15 m appears to fit the concentration differences best in monitor wells sampled in September 1994. It is assumed in this study that molecular diffusion is negligible with respect to advection and dispersion.

From field data and speciation-solubility modeling, Zhu et al. (2001) concluded that the distinct geochemistry zones in the aquifer could be interpreted with successive pH buffer reactions with calcite, amorphous $\text{Al}(\text{OH})_3$, and amorphous $\text{Fe}(\text{OH})_3$. This conceptual model was used as a geochemical submodel for the coupled reactive transport. A total of 11 aqueous components, H, Ca, Mg, Cl, CO_3^{2-} , Al, SO_4^{2-} , Fe^{3+} , Na, K, and Si, and six minerals, $\text{Al}(\text{OH})_3(\text{a})$, $\text{Fe}(\text{OH})_3(\text{a})$, calcite, gypsum, $\text{SiO}_2(\text{a})$, and illite, were included in the simulations. Equilibrium constants for chemical reactions are listed in Table 1. For simplicity, chemical reactions were calculated at 25 °C and 1 bar although measured groundwater temperatures range from 12 to 16 °C. The local equilibrium assumption (LEA) is used.

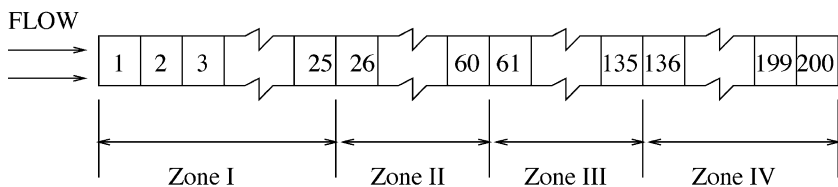


Fig. 3. Discretization of the simulated domain.

Table 1
Equilibrium constants used in the reactive transport model

Species	Reactions	Log <i>K</i>	Reference
FeOH ²⁺	Fe ³⁺ + H ₂ O = FeOH ²⁺ + H ⁺	-2.19	a
Fe(OH) ₂ ⁺	Fe ³⁺ + 2H ₂ O = Fe(OH) ₂ ⁺ + 2H ⁺	-5.67	a
Fe(OH) ₃ ⁰	Fe ³⁺ + 3H ₂ O = Fe(OH) ₃ ⁰ + 3H ⁺	-12.56	a
Fe(OH) ₄ ⁻	Fe ³⁺ + 4H ₂ O = Fe(OH) ₄ ⁻ + 4H ⁺	-21.6	a
Fe ₂ (OH) ₂ ⁴⁺	2Fe ³⁺ + 2H ₂ O = Fe ₂ (OH) ₂ ⁴⁺ + 2H ⁺	-2.95	a
Fe ₃ (OH) ₄ ⁵⁺	3Fe ³⁺ + 4H ₂ O = Fe ₃ (OH) ₄ ⁵⁺ + 4H ⁺	-6.3	a
AlOH ²⁺	Al ³⁺ + H ₂ O = AlOH ²⁺ + H ⁺	-5.0	a
Al(OH) ₂ ⁺	Al ³⁺ + 2H ₂ O = Al(OH) ₂ ⁺ + 2H ⁺	-10.1	a
Al(OH) ₃ ⁰ (aq)	Al ³⁺ + 3H ₂ O = Al(OH) ₃ ⁰ (aq) + 3H ⁺	-16.9	a
Al(OH) ₄ ⁻	Al ³⁺ + 4H ₂ O = Al(OH) ₄ ⁻ + 4H ⁺	-22.7	a
HCO ₃ ⁻	H ⁺ + CO ₃ ²⁻ = HCO ₃ ⁻	10.33	a
H ₂ CO ₃ ⁰ (aq)	CO ₃ ²⁻ + 2H ⁺ = H ₂ CO ₃ ⁰ (aq)	16.68	a
CaCO ₃ ⁰ (aq)	Ca ²⁺ + CO ₃ ²⁻ = CaCO ₃ ⁰ (aq)	3.22	a
CaHCO ₃ ⁻	Ca ²⁺ + CO ₃ ²⁻ + H ⁺ = CaHCO ₃ ⁻	11.44	a
HSO ₄ ⁻	SO ₄ ²⁻ + H ⁺ = HSO ₄ ⁻	1.99	a
CaSO ₄ ⁰ (aq)	Ca ²⁺ + SO ₄ ²⁻ = CaSO ₄ ⁰ (aq)	2.30	a
AlSO ₄ ⁺	Al ³⁺ + SO ₄ ²⁻ = AlSO ₄ ⁺	3.1	a
Al(SO ₄) ₂ ⁻	Al ³⁺ + 2SO ₄ ²⁻ = Al(SO ₄) ₂ ⁻	4.9	a
NaSO ₄ ⁻	Na ⁺ + SO ₄ ²⁻ = NaSO ₄ ⁻	0.07	a
CaCO ₃ (s)	Ca ²⁺ + CO ₃ ²⁻ = CaCO ₃ (s)	8.48	a
CaSO ₄ ·2H ₂ O (gypsum)	Ca ²⁺ + SO ₄ ²⁻ + 2H ₂ O = CaSO ₄ ·2H ₂ O	4.58	a
Illite	K _{0.6} Mg _{0.25} Al _{2.3} Si _{3.5} O ₁₀ (OH) ₂ + 11.2H ₂ O = 0.6K ⁺ + 0.25Mg ⁺² + 2.3Al(OH) ₄ ⁻ + 3.5H ₄ SiO ₄ + 1.2H ⁺	-40.267	a
SiO ₂ (a)	SiO ₂ (a) + 2H ₂ O = H ₄ SiO ₄	-2.71	a
Fe(OH) ₃ (a)	Fe ³⁺ + 3H ₂ O = Fe(OH) ₃ (a) + 3H ⁺	-4.89	b
Al(OH) ₃ (a)	Al ³⁺ + 3H ₂ O = Al(OH) ₃ (a) + 3H ⁺	-10.8	b

(a) Nordstrom et al. (1990).

(b) log *K* values from Ref. (a) were modified by adding 1.69 and subtracting 1.36 for Fe(OH)₃(a) and Al(OH)₃(a), respectively, to reflect site conditions assuming Fe and Al concentrations measured in groundwater were at equilibrium with these phases.

Initial conditions were specified to reflect site conditions in 1994. The domain was divided into four zones (Fig. 3), reflecting groundwater geochemical zonations observed in the field (Zhu et al., 2001). The pore fluid chemistry and aquifer mineral compositions for each zone are tabulated in Table 2. While the pore fluid chemistry was analyzed in September 1994, mineral compositions of the aquifer matrix were derived indirectly (Zhu et al., 2001). Alluvium deposits in the area unaffected by acid seepage have a neutralization capacity of up to 0.92 mol/l calcite equivalent. To be conservative, a 0.2 mol/l of calcite was used in the model. A value of 0.2 mol/l Fe(OH)₃(a) was assigned to Zone I. Background Fe(OH)₃(a) in the aquifer (Zones II, III, and IV) were assumed to be 0.05 mol/l, approximately 10% of the measured total iron (0.4 wt.%) in the Wasatch sandstones. Additionally, 0.1 mol/l Al(OH)₃(a) was assigned to Zone II and a value of 0.01 mol/l was assumed for the background (Zones III and IV). A 0.2 mol/l gypsum is assigned for both Zones I and II.

Table 2
Initial conditions for the reactive transport model

Zone	I	II	III	IV
Length	100 m	140 m	300 m	260 m
Cells	1–25	26–60	61–135	136–200
Pore water	TS-3	MW-86	MW-15	MW-12
Temp. (°C)	25	25	25	25
pH	3.8	4.5	6.5	6.7
Ca ²⁺	7.91×10^{-3}	1.06×10^{-2}	1.63×10^{-2}	1.38×10^{-2}
Mg ²⁺	4.21×10^{-2}	2.91×10^{-2}	1.03×10^{-2}	6.19×10^{-3}
HCO ₃ ⁻	1.06×10^{-4}	1.04×10^{-4}	2.91×10^{-2}	1.76×10^{-2}
Al ³⁺	3.87×10^{-2}	8.62×10^{-3}	4.95×10^{-5}	4.28×10^{-5}
SO ₄ ²⁻	1.76×10^{-1}	8.53×10^{-2}	1.73×10^{-2}	1.33×10^{-2}
Fe ³⁺	3.57×10^{-2}	1.68×10^{-3}	3.92×10^{-5}	1.24×10^{-5}
SiO ₂	6.89×10^{-4}	1.68×10^{-4}	1.62×10^{-4}	1.40×10^{-4}
K ⁺	1.57×10^{-3}	1.09×10^{-3}	4.63×10^{-4}	3.59×10^{-4}
Cl ⁻	1.59×10^{-2}	1.14×10^{-2}	1.06×10^{-2}	7.79×10^{-3}
Na ⁺	8.05×10^{-2}	4.95×10^{-2}	9.26×10^{-3}	1.16×10^{-2}
Minerals (mol/l)				
Al(OH) ₃ (a)	0, u	0.1	0.01	0.01
Gypsum	0.2	0.2	0, s	0, s
SiO ₂ (a)	0, u	0, u	0, u	0, u
Illite	0, u	0, u	0, s	0, s
Fe(OH) ₃ (a)	0.2	0.05	0.05	0.05
Calcite	0, u	0, u	0.2	0.2

Ground water flows from cell 1 to 200; Concentrations for pore fluids and solids are in mol/l, except for pH and temperatures; u: unsaturated; s: saturated.

Cauchy flux boundary conditions are used for both ends of the 1D strip. To represent the reclamation conditions, the incoming fluid has the chemistry of tailings pore fluid for the first 5 years and of uncontaminated upgradient groundwater thereafter (Table 3).

The advection, dispersion, and reaction of the 11 components under the above initial and boundary conditions was simulated by using PHREEQC Version 2.0, a one-dimensional finite-difference model. The advection–dispersion reaction (ADR) equation,

$$\frac{\partial C}{\partial t} = D_L \frac{\partial^2 C}{\partial x^2} - \bar{v} \frac{\partial C}{\partial x} - \frac{\rho_b}{\theta} \frac{\partial S}{\partial t}, \quad (1)$$

was solved, where C and S represent concentrations in fluid and solid matrix, respectively, t denotes time (T), x distance (L), ρ_b the bulk density of the aquifer (M/L^3), and θ the effective porosity. \bar{v} stands for the average linear velocity of groundwater (M/L) and D_L the longitudinal hydrodynamic dispersion coefficient (L^2/T) that is described by Bear (1972)

$$D_L = \bar{v} \alpha_L + D^0 \tau, \quad (2)$$

Table 3
Cauchy boundary fluxes used in the simulations

Concentrations (mol/l)	First 5 years TS-3	After 5 years MW-36
Temp. (°C)	25	25
pH	3.8	7.4
Ca ²⁺	7.91×10^{-3}	3.95×10^{-3}
Mg ²⁺	4.21×10^{-2}	8.65×10^{-4}
HCO ₃ ⁻	1.06×10^{-4}	2.51×10^{-3}
Al ³⁺	3.87×10^{-2}	3.71×10^{-7}
SO ₄ ²⁻	1.76×10^{-1}	4.43×10^{-3}
Fe ³⁺	3.57×10^{-2}	1.79×10^{-6}
SiO ₂	6.89×10^{-4}	9.33×10^{-5}
K ⁺	1.57×10^{-3}	1.79×10^{-4}
Cl ⁻	1.59×10^{-2}	1.26×10^{-3}
Na ⁺	8.05×10^{-2}	2.66×10^{-3}

where α_L stands for longitudinal dispersivity (L). D^0 and τ represent molecular diffusion coefficient (L²/T) and tortuosity (dimensionless), respectively. The reaction term, $(\rho_b/\theta)(\partial S/\partial t)$, is solved separately for each cell by using a chemical module, in which chemical speciation and partitioning between the solid matrix (including mineral surfaces) and aqueous solutions are calculated based on the mass-balance and mass-action equations (see Parkhurst, 1995).

In PHREEQC, a split-operator scheme is used to solve the advective and dispersive transport at consecutive stages. Within each time step, the advective transport is calculated first by using an upwind finite difference scheme. This is followed immediately by a calculation of chemical reactions. Then, dispersive transport is calculated using a central difference scheme (or mixing cell method, see Appelo and Postma, 1994). This is again followed by a calculation of chemical reactions. No iterations between the physical and chemical steps are used (cf. Yeh and Tripathi, 1989; Walter et al., 1994a; Steefel and MacQuarrie, 1996).

It is worthwhile noting that the time step for advection is determined by

$$\Delta t_A = \frac{\Delta x}{v}, \quad (3)$$

where Δx denotes the grid size. Eq. (3) ensures the satisfaction of the Courant–Fridrich–Lewy condition (i.e., $\Delta t_A \leq \Delta x/v$). As a result, the upwind scheme for advective transport gives exact results and thus eliminates numerical dispersion errors.

In PHREEQC, the von Neumann stability condition used for the dispersive transport is

$$D_L \frac{\Delta t_D}{\Delta x^2} \leq \frac{1}{3}, \quad (4)$$

which imposes an additional limitation of the time step for dispersion calculation, Δt_D . Condition (4) gives a much smaller time step than that of Eq. (3). The inconsistent

requirements by Eqs. (3) and (4) are resolved by using smaller time steps for dispersion calculations, so that

$$\Delta t_D = \frac{\Delta t_A}{N}, \quad (5)$$

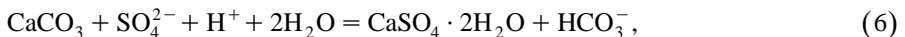
where N is an integer. Each of the N dispersion calculations is followed by chemical reaction calculations.

4. Analysis and discussion of numerical results

Simulations of reactive transport were performed for a period of 5 years of seepage by tailings fluids into the aquifer and 200 years of flushing of the plume by uncontaminated upgradient groundwater. Because this is a forward model, the modeling results are predictions of the future and cannot be compared to field data per se. However, for the seepage period, contamination of the aquifer is a continuation of the past and the same geochemical zonation progresses downgradient. Therefore, the simulated reaction sequence and concentration levels, although not associated with the spatial and temporal information, can be compared to field data. The observed solute concentrations and distributions have been analyzed using batch-scale geochemical modeling (Zhu et al., 2001). It is useful to compare them to the results of a model that incorporates transport. For the flushing period, there are no field data available for comparison presently, but modeling results can be compared to field data collected in the future.

4.1. Seepage of tailings fluids

The seepage of acidic tailings fluid into the shallow contaminated aquifer causes continued development of geochemical zonations corresponding to the successive buffer reactions with calcite, $\text{Al(OH)}_3(\text{a})$, and $\text{Fe(OH)}_3(\text{a})$. The pH of groundwater is buffered to 6.3, 4.3, and 3.8, respectively. The reaction



has a log K value of 6.33 at 25 °C and 1 bar. The buffered pH value by this reaction is determined by the ratios of the activity of HCO_3^- and SO_4^{2-} ,

$$\text{pH} = \log K_{10} - \log \left(\frac{a_{\text{HCO}_3^-}}{a_{\text{SO}_4^{2-}}} \right). \quad (7)$$

At the calcite dissolution front, activities of HCO_3^- and SO_4^{2-} are close to being equal, and, hence, the pH is buffered to 6.3.

The reaction,



buffers groundwater pH to about 4.3 and the reaction,



controls groundwater pH to about 3.8. The reaction fronts and geochemical zones shift downgradient with time. These predicted pH values are generally consistent with field data (Zhu et al., 2001).

Numerical simulations show that the dissolution of calcite (Fig. 4) causes a sharp rise of total dissolved inorganic carbon (DIC) concentrations at the reaction front. This front dissipates downstream. This compares well with the field data, as seen in a value as high

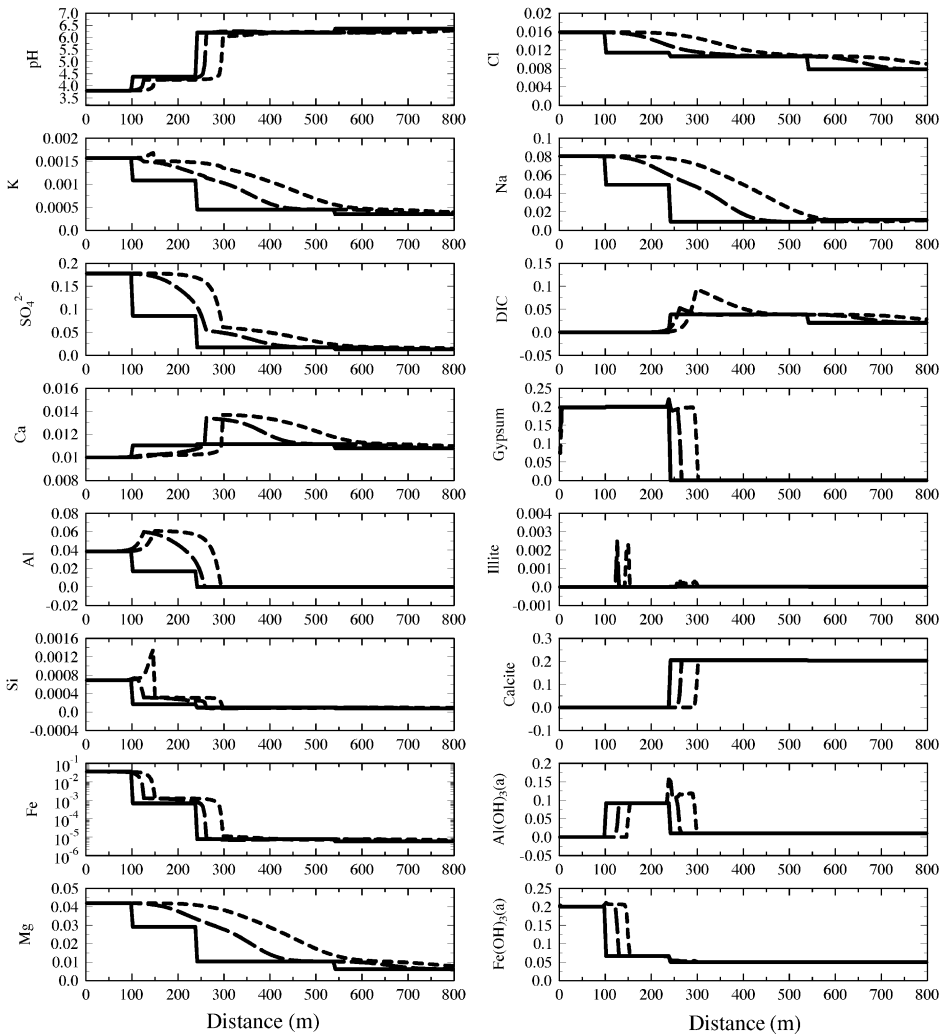


Fig. 4. Concentration profiles showing downgradient propagation of the reaction fronts and pH-buffered geochemical zones during tailings fluid intrusion. Groundwater flows from left to right. DIC denotes total dissolved inorganic carbon. All concentration units are in mol/l, except for pH. Solid, dashed, and dotted lines represent concentration profiles at 0, 2.5, 5 years from the start of the simulation, respectively.

as 0.029 mol/l of HCO_3^- in the area immediate downstream from the plume (Zhu et al., 2001). Areas further downstream (e.g., MW-14, Fig. 1) where the pH values are still close to background level (MW-36 in Fig. 1) have DIC as large as twice the background.

The predicted Al^{3+} concentrations show a sharp drop at the calcite dissolution front, corresponding to the sharp rise of pH. Near the inlet, $\text{Al}(\text{OH})_3(\text{a})$ is dissolved by the intruding tailings fluid (Fig. 4). $\text{Al}(\text{OH})_3(\text{a})$ is dissolved at the upstream end and accumulates at the downstream end of the $\text{Al}(\text{OH})_3(\text{a})$ zone. The zone moves downstream as the seepage continues.

The transport and reactions for Fe^{3+} have a similar pattern to Al^{3+} (Fig. 4). Fe^{3+} is first reduced to the level of 10^{-3} mol/l at the interface with $\text{Al}(\text{OH})_3(\text{a})$, and then reduced to 10^{-5} mol/l level at the calcite dissolution front, in response to sharp pH rise. Downstream from the calcite dissolution front, Fe^{3+} concentrations are nearly constant. This prediction is consistent with field data (e.g., MW-86 and MW-15).

Accompanied with calcite dissolution, gypsum is precipitated from groundwater and sulfate concentrations are reduced sharply (Fig. 4). The gypsum zone advances downstream at the same rate as that of the calcite dissolution front.

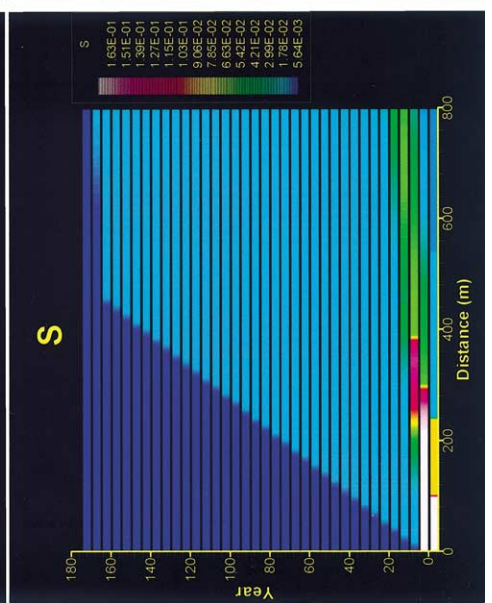
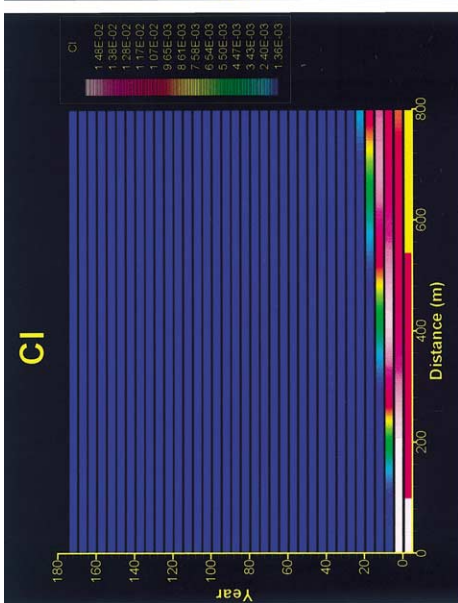
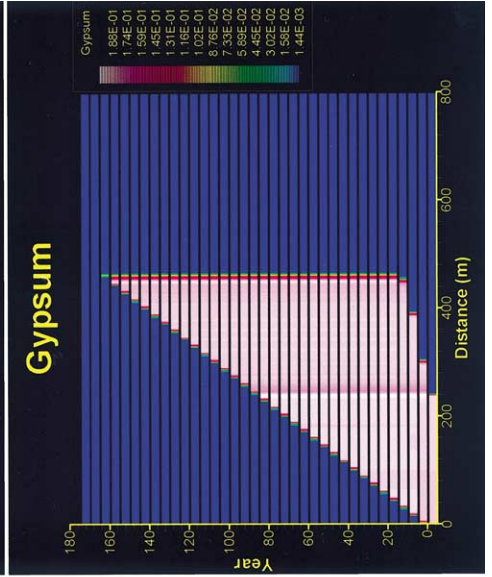
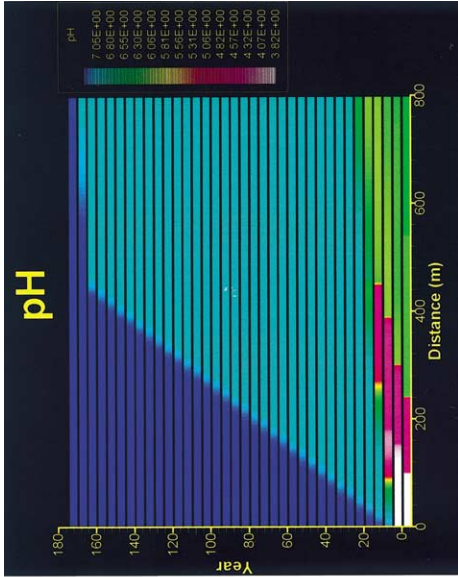
The numerical simulation predicts illite precipitation but no amorphous silica precipitation. Illite occurs at the $\text{Al}(\text{OH})_3(\text{a})$ dissolution front as a single sharp peak, and a flat peak at the calcite dissolution front. This occurrence corresponds to higher pH and Al^{3+} concentrations at the $\text{Al}(\text{OH})_3(\text{a})$ front. As illite is precipitated, aqueous silica concentrations drop threefold (Fig. 4). Such a decrease is seen in the field data and laboratory neutralization experiments (Zhu et al., 2001).

The precipitation of illite only marginally affects K^+ concentrations and has no discernible effects on Mg^{2+} concentrations (Fig. 4). In laboratory neutralization experiments of tailings fluids, the concentrations of Mg^{2+} and K^+ do not decrease (see discussion in Zhu et al., 2001). The decrease seen in field data can be either advective–dispersive transport or reactions with aquifer minerals or both. However, there are insufficient field data to show whether the decrease is gradual or as sharp fronts. Field data show an increase of Na^+ from the calcite dissolution front (and hence the higher Ca^{2+} concentration front), which may result from Ca–Na or Mg–Na exchange reactions, which is common in sediment aquifers. However, Na^+ is not included in any minerals in the model and essentially is modeled as a conservative tracer in this study.

4.2. Flushing by upgradient groundwater

Numerical simulation predicted several stages of geochemical evolution. First, the entrained acidic water in the pores continues to move downstream and the set of reactions begun during the seepage period continues. Second, dissolution of gypsum occurs because the incoming groundwater is undersaturated with it. Third, when all gypsum in the plume is expended, groundwater returns to background concentrations after a short period of perturbation.

Chemical reactions and advection–dispersion alternatively dominate the transport of reactive constituents. For example, pH fronts first continue to advance downstream because of the entrained acid in pore water (Fig. 5). The dissolution of gypsum near the



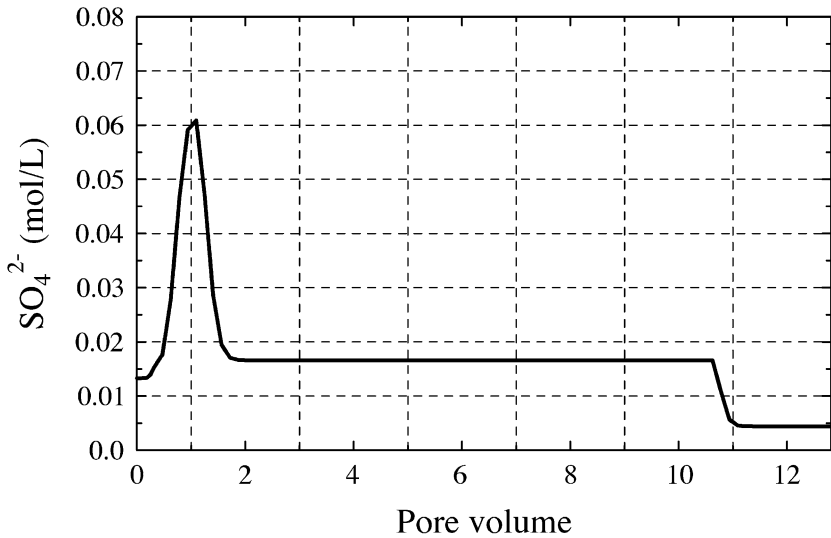


Fig. 6. Breakthrough curves for sulfate concentrations in 200th cell, showing multiple concentration fronts. The long concentration plateau shows SO_4^{2-} concentrations controlled by equilibrium with gypsum, even though no gypsum is present in the cell or cells immediately upstream, conforming to the downstream equilibrium condition.

inlet causes an increase in Ca^{2+} concentration, precipitation of calcite, and a drop of pH through reaction (6), which now proceeds in the opposite direction. The pH is buffered to a higher value of 7 (vs. 6.3), because the activity ratios of bicarbonate to sulfate are lower. Downstream from the gypsum dissolution fronts, higher pH fluid (about 6.9) from upgradient mixes with lower pH pore fluid (about 6.4), which produces an advective–dispersive transport front that is similar to a front for conservative solutes. pH increases again after all gypsum in the aquifer is dissolved at about 165 year of flushing (Fig. 5). The pH of downstream pore water again has advective–dispersive curves for conservative tracers. pH is returned to background value after about 172 years of flushing.

Sulfate concentrations are controlled by gypsum dissolution. After the seepage concentrations dissipate, sulfate downstream of the gypsum dissolution front is controlled by the equilibrium concentration with respect to gypsum. Gypsum is completely expended after 165 year of flushing. The sulfate concentrations return to background concentration in about 172 years (Fig. 5). Sulfate breakthrough in the last cell of the 1D domain is shown in Fig. 6. A concentration peak associated with the advective–dispersive front is followed by a concentration plateau reflecting equilibrium with gypsum.

Fig. 5. Time–distance concentration distributions showing multiple and coherent waves as a result of attenuation reactions in the aquifer. A different sequence of reactions occurs during tailings fluid intrusion and flushing by uncontaminated groundwater.

Here, no gypsum is present in the cell or cells immediately upstream so that the “downstream equilibrium condition” is observed. When gypsum was expended, SO_4^{2-} concentrations decreased to the background level.

4.3. Analysis of concentration wave propagation

The numerical modeling results are plotted in the time–space concentration distribution diagrams (Figs. 5 and 7) and analyzed using wave propagation theories. In these diagrams, the flushing started at year 0 and the concentration distributions in the seepage period are shown in the negative time domain. Distinct concentration waves or fronts are seen in these diagrams. Helfferich (1989) defined “wave” as any variation of solute or solid phase concentration and is synonymous with “front.” For the convenience of discussion, constant concentration levels for SO_4^{2-} and gypsum have been traced and plotted in Fig. 7.

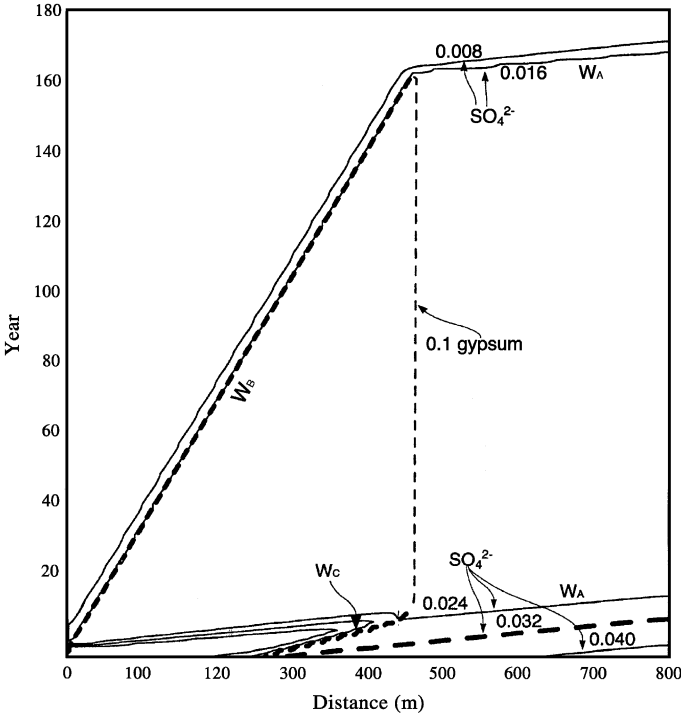


Fig. 7. Concentration waves for SO_4^{2-} . The lines are constant concentration levels as labeled in mol/l: solid lines for SO_4^{2-} and thin dashed line for gypsum. In this distance vs. time plot, the slopes of the lines represent the speeds of wave propagation. The steeper the slope, the slower the movement of that wave. SO_4^{2-} concentration waves propagate downgradient in three different speeds in different time–space domains, represented by thick dashed lines. W_A , advective–dispersive wave. Note there are several equal concentration lines that have approximately the same slope; W_B , gypsum dissolution wave; W_C , gypsum precipitation wave.

The first type of wave for SO_4^{2-} transport is the advection–dispersion wave, denoted as W_A in Fig. 7. It has a propagation velocity equal to that of the pore fluid (50 m/year). The concentrations are smoothly diffused near the wavefront due to the dispersion included in the model. This type of wave is referred to as a “salinity” wave (Bryant et al., 1987; Schweich et al., 1993). For solutes modeled as conservative tracers, namely Na^+ and Cl^- , salinity waves are the only wave type for them (see Fig. 5 for Cl^-).

The second type of wave is the gypsum-dissolution wave, denoted as W_B in Fig. 7. Chemically, this wave represents the front of higher SO_4^{2-} concentrations due to the dissolution of gypsum by uncontaminated upstream groundwater. The velocity of this wave is less than that of the pore fluid. Measurement of the wavefronts from numerical simulation indicates a speed of about 2.83 m/year. It is important to note that the Ca^{2+} , SO_4^{2-} , calcite precipitation, and pH decrease fronts that are involved in the gypsum dissolution process propagate at the same velocity, exhibiting a “coherent” wave structure (Helfferich and Klein, 1970; Walsh et al., 1984). After all gypsum has been dissolved at about 165 years flushing, SO_4^{2-} propagates at the velocity of the advection–dispersion wave as shown in Fig. 7.

The third type of wave is the calcite dissolution and gypsum-precipitation wave, denoted as W_C in Fig. 7. The calcite dissolution and gypsum precipitation waves are coherent with each other and coherent with the front of higher SO_4^{2-} concentration because of the seepage of acidic tailings fluids. As shown in Fig. 7, the gypsum-precipitation wave propagates at a speed faster than the gypsum-dissolution wave (W_B). As a result, the gypsum region widens as the flushing time increases until precipitation ends. Measured from the computed wavefronts, the gypsum-precipitation wave has a speed of 16.36 m/year. Again, all components involved (Ca^{2+} , SO_4^{2-} , pH, and CO_3^{2-}) propagate at the same speed and coherence is observed.

The speeds of the above wave types are calculated analytically and compared to numerical simulation results in Appendix A. It is shown in Appendix A that, when concentration plateaus exist at both sides of a concentration front, the wave speeds are independent from hydrodynamic dispersion. Hence, the analytical solution for calculating wave propagation speeds under advection and local equilibrium conditions (Helfferich and Klein, 1970) can be used to estimate, approximately, the wave speeds in the presence of hydrodynamic dispersion. Calculations using this analytical solution (see Appendix A) show that the velocity of the calcite dissolution front is faster than the gypsum dissolution front because Ca^{2+} is present in solids at both sides of the dissolution wavefront (calcite at the downstream and gypsum at the upstream) and the two solids have approximately equal mole concentrations. For the gypsum dissolution wave, only a trace amount of calcite precipitates at the upstream side ($\sim 10^{-6}$ mol/l), but a large amount of gypsum (0.2 mol/l) exists at the downstream side of the wave. Wave speeds calculated from analytical solutions for gypsum dissolution and calcite dissolution are 2.83 and 17.16 m/year, which compare well with measured speeds from numerical modeling results of 2.82 and 16.36 m/year, respectively. Thus, numerical simulations produce results that are consistent with analytical solutions. The simulated results where the calcite dissolution wave moves faster than the gypsum dissolution wave are also consistent with chemical arguments. Precipitation of gypsum removes Ca^{2+} from the aqueous solution and creates lower Ca chemical energy barriers, on the Ca^{2+}

activity part, favoring more calcite dissolution. The quantity of calcite that can be dissolved depends on the advective–dispersive dissipation of the CO_3^{2-} . It shows that in a reactive flow regime, the interplay of reactions and physical transport is significant even when a local equilibrium condition is assumed.

4.4. Sensitivity analysis and model limitations

Sensitivity analysis was conducted by varying hydraulic and geochemical parameters for the seepage simulations. When all other parameters remain unchanged, higher flow velocity would push the reaction fronts further downstream simply because more pore volumes of tailings fluid have reacted with the aquifer matrix.

The effects of dispersivity on reactive transport were evaluated by varying longitudinal dispersivity, α_L , from 10 to 0 and 80 m. With an α_L of 80 m, the reaction fronts spread further downstream. The gypsum and $\text{Al}(\text{OH})_3(\text{a})$ precipitation zones spread significantly broader toward downstream. As expected, conservative solutes spread out further with larger α_L values.

Sensitivity analysis was also conducted by varying initial mineral concentrations in the aquifer matrix and by including surface complexation reactions. The initial conditions have a significant impact on the distance of plume migration and duration of natural attenuation. As stated in the Introduction, the purpose of this study is not to find an answer for this site, but to explore the intricate interplay between physical transport and chemical reactions. Therefore, although the initial mineral concentrations are significant to practical concerns for the site, they do not alter the patterns of geochemical evolution. Different mineral reactions in the geochemical model also change the modeling results. Inclusion of surface reactions does not significantly change the reactive transport in the seepage period, but significantly increases acidity in the plume. These reaction patterns are quite complex and are the subject of ongoing research.

Despite their complexity, the present model results are far from a complete answer to the problem in this area, but they are a step in the right direction. One of the advantages of numerical modeling is that important factors, which are poorly known or unknown, can be revealed. We also realize that it is prudent to build our knowledge in a phased approach from simple to more complex models. Hence, this study only dealt with the migration of major groundwater constituents. The model limitations are obvious:

(1) A uniform and constant Darcy velocity was assumed whereas drainage of tailings fluid in the aquifer changes hydraulic gradients. The negligence of mixing of water from both sides of the alluvium channel along the 1D domain probably resulted in an underestimation of the dilution effect.

(2) The local equilibrium assumption was used (Knapp, 1989). However, reactions that are known to be controlled by kinetics such as feldspar dissolution and quartz precipitation were not included in the model. The use of illite as an equilibrium phase and the sink for $\text{SiO}_2(\text{aq})$ is not well supported by field evidence, although illite precipitation has negligible effects in the overall modeling results.

(3) The porosity of the porous media is constant during flow. Thus, the reactive solids only occupy small fractions of the bulk media. Dissolution and precipitation of 0.2

mol/l gypsum would change about 1.5% porosity. The simulations assumed that it has negligible effects on the transport.

(4) The precipitates are stationary, e.g., precipitates are not transported with the flow as colloids. It is possible that amorphous Fe and Al hydroxides form colloidal materials in the aquifer.

(5) TDS contents in the tailings fluids and background water are significantly different. Thus, the density of fluids may have significant effect on solute transport.

(6) The actual mineral assemblage, both primary and secondary, their relative abundances, and spatial distributions are very important to the modeling results. However, no detailed mineralogical data are available.

(7) More chemical reactions like cation exchange and surface reactions may be operative in the field but neglected in the model.

5. Summary and conclusions

The migration of major groundwater constituents under a reclamation scenario of a uranium mill tailings impoundment was simulated using the reactive mass transport model PHREEQC. A detailed geochemical model was included in the transport simulation. Two types of conditions were simulated: seepage of acidic tailings fluid into a shallow sandy aquifer and flushing by upgradient uncontaminated groundwater after the source of contamination is terminated. Each of the conditions produced a set of chemical reaction and transport patterns that are typical for acid mine drainage contamination of an aquifer or a remediation/natural attenuation scheme. Therefore, the results of simulation have general implications for acid mine drainage problems.

The simulations show that:

(1) For acidic tailings fluid seepage condition, the numerical model predicted SO_4^{2-} , Ca^{2+} , Fe^{3+} , Al^{3+} , CO_3^{2-} , and H^+ distributions in distinct geochemical zones, controlled by pH buffer reactions with calcite, $\text{Al}(\text{OH})_3(\text{a})$, and $\text{Fe}(\text{OH})_3(\text{a})$, respectively. Simulated pattern, sequence, and concentration levels are comparable to field data although the forward model cannot be compared to the spatial and temporal information in the field. Most mass transfer reactions occur at the interfaces of different geochemical zones. Hence, the successive pH buffer reaction model of Zhu et al. (2001), inferred from field data and batch-scale static geochemical modeling, appears to interpret successfully the field data when transport processes are included in simulations. This transport and reaction pattern should be general for all acid mine drainage systems where calcite is present.

(2) Numerical modeling predicts several stages of geochemical evolution during the flushing of contaminated sediments by uncontaminated upgradient groundwater. Gypsum dissolution drives the pH, SO_4^{2-} , and Ca^{2+} concentration distributions and this was followed by advective–dispersive transport. The duration of natural attenuation depends on the initial conditions in the model. This dependence remains to be investigated. Model predictions can also be assessed by examining monitoring data at this site in the future.

(3) In different time–space domains, the transport of reactive constituents is dominated alternatively by chemical reactions or physical transport processes, which produces multiple concentration waves that have different speeds. In the case of SO_4^{2-} , the waves are controlled by advection–dispersion, gypsum precipitation, gypsum dissolution, and then advective–dispersive transport, in a sequence. “Coherent” waves for different constituents were also produced. Simulated wave speeds compare well to those calculated from an analytical solution.

Acknowledgements

We are indebted to Gary Chase and Ernie Scott of Awadarko Petroleum Corporation for their permission to use the site data to conduct research and publication of the results and to David Parkhurst and Tony Appelo for discussions on the use of PHREEQC 2.0. We thank Greg Anderson, Martin Appold, Karen Salvage, Frank Schwartz, and Motomu Ibaraki for review of the manuscript. Although the research described in this article has been funded wholly or in part by US Environmental Protection Agency, it has not been subject to the Agency’s review and therefore does not necessarily reflect the views of the Agency, and no official endorsement should be inferred. Permission by Union Pacific Resources for publishing the modeling results does not necessarily reflect their agreement with the approaches or parameters used in the model or model predictions. Assistance from Dana McClish in various aspects of this work is greatly appreciated.

Appendix A. A note on the wave propagation speed in the presence of dispersion

In this appendix, we consider the propagation speed of the precipitation and dissolution waves in the presence of dispersivity and give an approximate solution for estimating the wave speed.

When dispersion is not present, the precipitation and dissolution wavefronts are sharp and their propagation speeds have been derived and given in the literature (e.g., Helfferich and Klein, 1970). The speed of the wave is related to the jump conditions across the wavefront. When dispersion is present, concentration changes are more gradual near the wavefronts as seen in our calculations. We will show, however, that the wave speed can still be related to the values of concentrations across the wavefront under the conditions given below.

Our numerical calculations indicate that, in many cases, concentration plateau zones are still formed in the presence of dispersion, as illustrated in Fig. 8. Our discussions will be based on the assumption that concentrations are constant, or nearly constant, upstream and downstream of the wave zone. In addition, we also assume that the pore velocity \bar{v} and dispersivity D_L are constant, as in our numerical calculations. To facilitate our discussions, we will define the location of a wavefront x_s such that the shaded areas in Fig. 8 are the same.

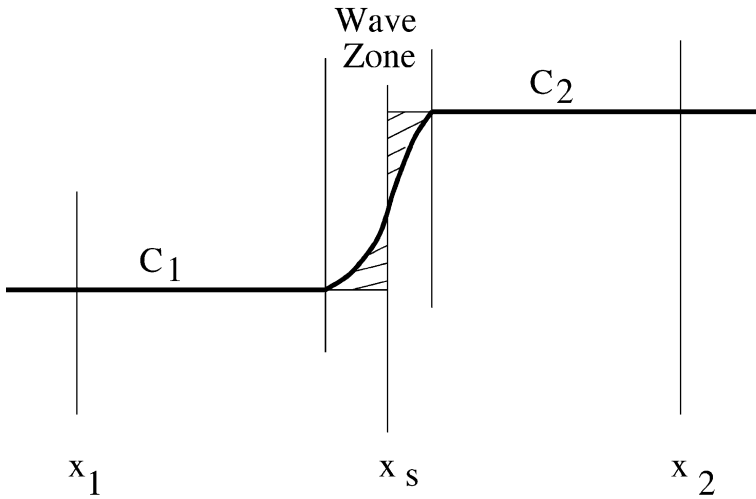


Fig. 8. A schematic diagram showing the wave zone and concentration plateau zones.

The propagation of component C is governed by the advection–dispersion reaction equation

$$\frac{\partial C^a}{\partial t} + \frac{\partial C^s}{\partial t} + \bar{v} \frac{\partial C^a}{\partial x} + D_L \frac{\partial^2 C^a}{\partial x^2} = 0, \tag{A1}$$

where C^a and C^s are the concentrations in the aqueous and solid phases, respectively. To find the wave speed, integrate the equation across the wavefront from a fixed location upstream at x_1 to a fixed location downstream at x_2 , as shown in Fig. 8:

$$\frac{\partial}{\partial t} \int_{x_1}^{x_2} C^a dx + \frac{\partial}{\partial t} \int_{x_1}^{x_2} C^s dx + \bar{v} \int_{x_1}^{x_2} \frac{\partial C^a}{\partial x} dx + D_L \int_{x_1}^{x_2} \frac{\partial^2 C^a}{\partial x^2} dx = 0. \tag{A2}$$

The third and fourth terms in Eq. (A2) can be integrated immediately and Eq. (A2) becomes

$$\frac{\partial}{\partial t} \int_{x_1}^{x_2} C^a dx + \frac{\partial}{\partial t} \int_{x_1}^{x_2} C^s dx + \bar{v} (C_2^a - C_1^a) + D_L \left(\left. \frac{\partial C^a}{\partial x} \right|_{x_2} - \left. \frac{\partial C^a}{\partial x} \right|_{x_1} \right) = 0, \tag{A3}$$

in which subscripts indicate the values upstream and downstream of the wavefront, respectively. Since we have assumed that aqueous concentrations are constant or nearly constant at x_1 and x_2 , the fourth term above will be zero or approximately zero and will be neglected. Furthermore, using the wavefront location x_s , the integrals in the first and second terms in Eq. (A2) can be evaluated as follows:

$$\int_{x_1}^{x_2} C^a dx = C_1^a (x_s - x_1) + C_2^a (x_2 - x_s),$$

$$\int_{x_1}^{x_2} C^s dx = C_1^s (x_s - x_1) + C_2^s (x_2 - x_s).$$

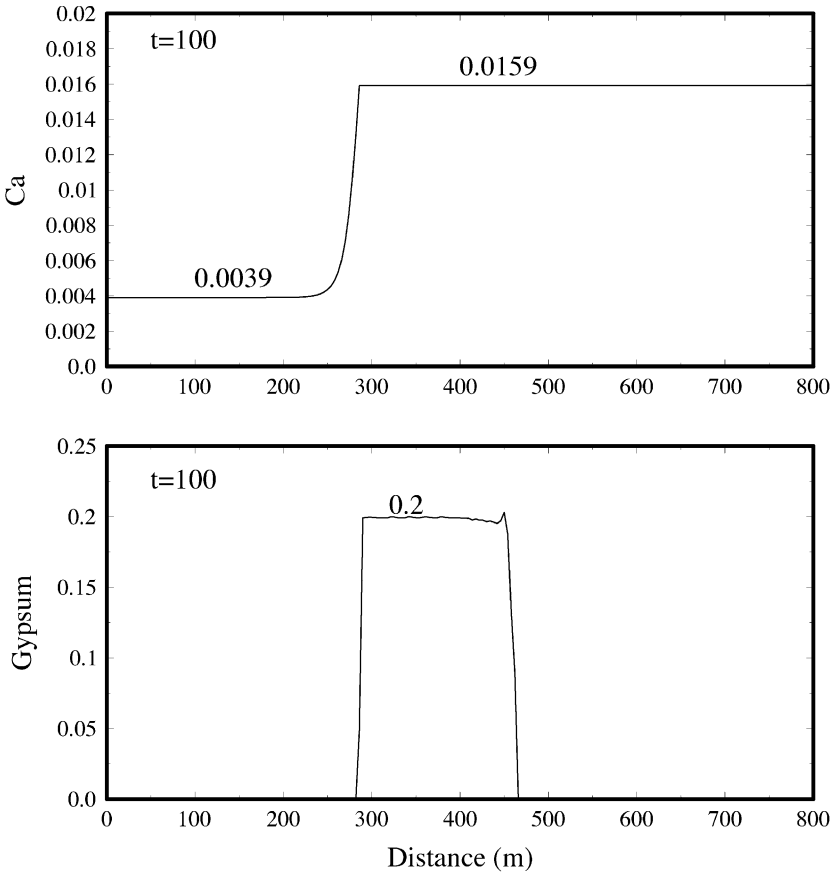


Fig. 9. Concentration profiles of dissolved Ca^{2+} and gypsum at $t = 100$ (year), showing the gypsum-dissolution wave.

Consequently, Eq. (A3) becomes

$$(C_1^a - C_2^a) \frac{\partial x_s}{\partial t} + (C_1^s - C_2^s) \frac{\partial x_s}{\partial t} + \bar{v}(C_2^a - C_1^a) = 0,$$

since x_1 and x_2 are fixed and their time derivatives are zero. Thus, we get the wave speed for the wavefront

$$\frac{\partial x_s}{\partial t} = \bar{v} \frac{C_2^a - C_1^a}{(C_2^a - C_1^a) + (C_2^s - C_1^s)}, \tag{A4}$$

or

$$\frac{\partial x_s}{\partial t} = \bar{v} \frac{C_2^a - C_1^a}{C_2^T - C_1^T}, \tag{A5}$$

where C^T is the total concentration of the component in both the aqueous and solid phases. We note that the above formula is the same as those derived for waves when dispersion is not present (Helfferich and Klein, 1970). It shows that this formula is still applicable as long as concentration plateau zones are formed adjacent to a wavefront. When concentration plateau zones are not formed, as we have seen in our numerical simulations for some components, Eq. (A5) is not accurate.

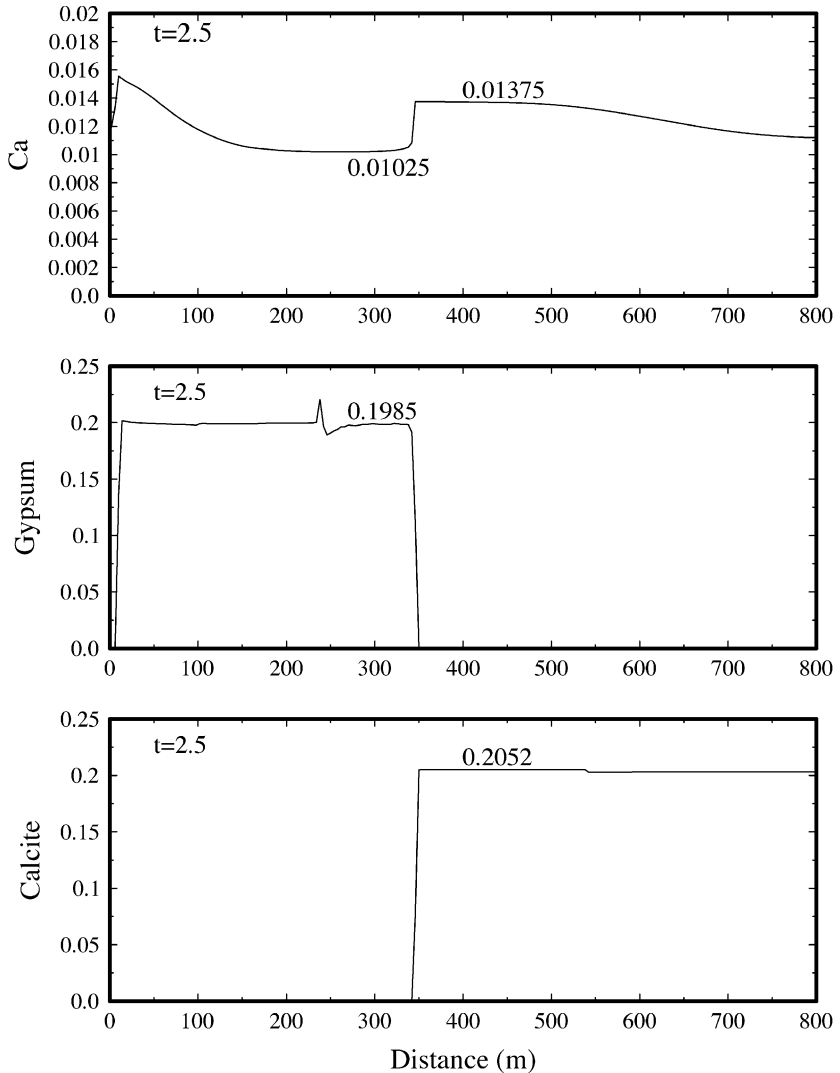


Fig. 10. Concentration profiles of dissolved Ca^{2+} , gypsum and calcite at $t = 2.5$ (year), showing the calcite-dissolution and gypsum-precipitation wave.

To demonstrate the validity of Eq. (A5), two examples from our numerical results will be shown below.

First, consider the gypsum dissolution wave (W_B in Fig. 7), using Ca^{2+} concentration for calculation. Profiles of relevant distributions are plotted in Fig. 9 with indicated plateau values. Here, we have $\bar{v} = 50$ (m/year) and

$$C_1^a = 0.0039, \quad C_1^T = 0.0039$$

$$C_2^a = 0.0159, \quad C_2^T = 0.0039 + 0.2 = 0.2039$$

$$\text{wave speed} = 50 \frac{0.0159 - 0.0039}{0.2159 - 0.0039} = 2.83 \text{ (m/year)}$$

The measured wave speed from numerical simulation, shown in Fig. 7, is 2.82 m/year. A very good agreement is seen.

Second, consider the calcite-dissolution and gypsum-precipitation wave (W_C in Fig. 7). Profiles of the concentrations of Ca^{2+} , gypsum and calcite are shown in Fig. 10. Here, we have

$$C_1^a = 0.01025, \quad C_1^T = 0.01025 + 0.1985 = 0.2085$$

$$C_2^a = 0.01375, \quad C_2^T = 0.01375 + 0.2052 = 0.21895$$

$$\text{wave speed} = 50 \frac{0.01375 - 0.01025}{0.21895 - 0.2085} = 17.16 \text{ (m/year)}$$

The measured wave speed from numerical simulations is 16.36 m/year, a close agreement.

Finally, we note that precipitation and dissolution of solid phases can result in changes of pore velocities \bar{v} and dispersivity D_L . The condition of constant velocity and dispersivity may be least satisfied in the vicinity of a wavefront, but necessary for the derivation of Eq. (A5). Because this condition is the same for numerical simulations, the agreement between numerical and analytical results does not validate the applicability of Eq. (A5).

References

- Appelo, C.A.J., Postma, D., 1994. *Geochemistry, Groundwater, and Pollution*. Balema, Rotterdam.
- Bear, J., 1972. *Dynamics of Fluids in Porous Media*. Dover Publications, New York, NY.
- Bethke, C.M., Brady, P.V., 2000. How the Kd approach undermines ground water cleanup. *Ground Water* 38 (3), 435–443.
- Bryant, S.L., Schechter, R.S., Lake, L.W., 1987. Mineral sequences in precipitation/dissolution waves. *AIChE Journal* 33 (8), 1271–1287.
- Cederberg, G.A., Leckie, J.O., Street, R.L., 1985. A groundwater mass transport and equilibrium chemistry model for multicomponent systems. *Water Resource Research* 21, 1095–1104.
- Glynn, P., Brown, J., 1996. Reactive transport modeling of acid metal-contaminated groundwater at a site with

- sparse spatial information. In: Lichtner, P.C., Steefel, C.I., Oelkers, E.H. (Eds.), *Reactive Transport in Porous Media*. Review in Mineralogy, Mineralogical Society of America, Washington, DC.
- Helferich, F.G., 1989. The theory of precipitation/dissolution waves. *AIChE Journal* 35 (1), 75–87.
- Helferich, F.G., Klein, G., 1970. *Multicomponent Chromatography*. Marcel Dekker, New York, NY.
- King, T.V.V. (Ed.), 1995. *Environmental considerations of active and abandoned mine lands*. United States Geological Survey Bulletin, 2220.
- Knapp, R.A., 1989. Spatial and temporal scales of local equilibrium in dynamic fluid–rock systems. *Geochimica et Cosmochimica Acta* 53, 1955–1964.
- Lichtner, P., 1985. Continuum model for simultaneous chemical reactions and mass transport in hydrothermal systems. *Geochimica et Cosmochimica Acta* 49, 779–800.
- Mangold, D.C., Tsang, C.F., 1991. A summary of subsurface hydrological and hydrochemical models. *Reviews of Geophysics* 29, 51–79.
- Nordstrom, D.K., Busenberg, E., Jones, B.F., Langmuir, D., May, H.M., Parkhurst, D.L., Plummer, L.N., 1990. Revised chemical equilibrium data for major water–mineral reactions and their limitations. In: Bassett, R., Melchoir, D. (Eds.), *Chemical Modeling in Aqueous Systems II*. Am. Chem. Soc. Symp. Ser. 416, 398–413.
- Parkhurst, D.L., 1995. User's guide to PHREEQC—a computer program for speciation, reaction-path, advective-transport, and inverse geochemical modeling. U.S. Geological Survey, Water-Resource Investigation Report, pp. 95–4227.
- Parkhurst, D.L., Appello, A.A.J., 1999. User's guide to PHREEQC (version 2)—a computer program for speciation, batch-reaction, one dimensional transport, and inverse geochemical modeling. U.S. Geological Survey, Water-Resource Investigation Report, pp. 99–4259.
- Raffensperger, J.P., Garven, G., 1995. The formation of unconforming-type uranium ore deposit: 2. Coupled hydrochemical modeling. *American Journal of Science* 295, 581–636.
- Reardon, E.J., 1981. K_d 's—Can they be used to describe reversible ion sorption reactions in contaminant migration? *Ground Water* 19 (3), 279–286.
- Sharp, W.N., Gibbons, A.B., 1964. Geology and uranium deposits of the southern part of the Powder River basin, Wyoming. USGS Bulletin, 1147-D.
- Schwartz, F.W., Domenico, P.A., 1973. Simulation of hydrochemical patterns in regional groundwater flow. *Water Resources Research* 9, 1293–1297.
- Schweich, D., Sardin, M., Jauzein, M., 1993. Properties of concentration waves in presence of nonlinear sorption, precipitation/dissolution, and homogenous reactions: 1. Fundamentals. *Water Resource Research* 24, 723–733.
- Steefel, C., Lasaga, A., 1994. A coupled model for transport of multiple chemical species and kinetic precipitation/dissolution reactions with applications to reactive flow in single phase hydrothermal systems. *American Journal of Science* 294, 529–592.
- Steefel, C., MacQuarrie, K.T.B., 1996. Approaches to modeling of reactive transport in porous media. In: Lichtner, P.C., Steefel, C.I., Oelkers, E.H. (Eds.), *Reactive Transport in Porous Media*. Review in Mineralogy, Mineralogical Society of America, Washington, DC, pp. 83–130.
- Stumm, W., Morgan, J., 1981. *Aquatic Chemistry—Chemical Equilibria and Rates in Natural Waters*. Wiley, New York, NY.
- Walsh, M.P., 1983. *Geochemical Flow Modeling*. PhD dissertation, University of Texas, Austin, TX.
- Walsh, M.P., Bryant, S.L., Lake, L.W., Schechter, R.S., 1984. Precipitation and dissolution of solids attending flow through porous media. *AIChE Journal* 30 (2), 317–328.
- Walter, A.L., Blowes, D.W., Frind, E.O., Molson, J.W., Ptacek, C.J., 1994a. Modeling of multicomponent reactive transport in groundwater: 1. Model development and evaluation. *Water Resources Research* 30, 3137–3148.
- Walter, A.L., Blowes, D.W., Frind, E.O., Molson, J.W., Ptacek, C.J., 1994b. Modeling of multicomponent reactive transport in groundwater. 2. Metal mobility in aquifers impacted by acidic mine tailings discharge. *Water Resources Research* 30, 3149–3158.
- Yeh, G.T., Tripathi, V.S., 1989. A critical evaluation of recent development of hydrogeochemical transport models of reactive multi-components. *Water Resource Research* 25 (1), 93–108.
- Yeh, G.T., Tripathi, V.S., 1991. A model for simulating transport of reactive multispecies components: model development and demonstration. *Water Resource Research* 27 (12), 3075–3094.

- Zhu, C., Waddell, R.K., Yeh, G.T., 1996. TRANSRXN—a coupled geochemical model and hydrological model with coprecipitation for simulation of reactive transport in groundwater systems. Submitted to US EPA.
- Zhu, C., Anderson, G.M., Burden, D.S., 2001. Geochemical modeling of natural attenuation reactions in a contaminated shallow aquifer at a uranium mill tailings site, western USA. *Ground Water* (in press).